Supporting Information

Structural and Spectroscopic Evidence for a Side-on Fe(III)-superoxo Complex Featuring Discrete O-O Bond Distances

Hung-Ruei Pan,[†] Hsin-Jou Chen,[†] Zong-Han Wu,[†] Pu Ge,[‡] Shengfa Ye,[⊥,§,*] Gene-Hsiang Lee,[∥] Hua-Fen Hsu[†*]

[†]Department of Chemistry, National Cheng Kung University, Tainan 701, Taiwan

[‡]School of Environmental Science and Technology, Dalian University of Technology, Dalian, 116024, China

[⊥]State Key Laboratory of Catalysis, Dalian Institute of Chemical Physics, Chinese Academy of Sciences, Dalian 116023, China;

[§]Max-Planck-Institut für Kohlenforschung, Mülheim an der Ruhr D-45470, Germany

[∥]Department of Chemistry, National Taiwan University, Taipei 106, Taiwan

Corresponding author information

*Prof. H.-F. Hsu E-mail: konopka@mail.ncku.edu.tw

*Prof. S. Ye E-mail: shengfa.ye@dicp.ac.cn

Table of content

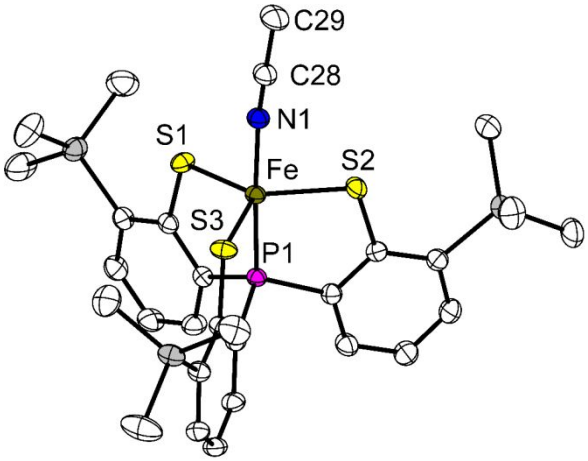

Figure S1. The ORTEP diagram of $[AsPh_4][Fe(PS3")(CH_3CN)]\cdot 5CH_3CN$ displaying with 35% thermal ellipsoid. The cation, solvated molecules and hydrogen atoms are omitted for the clarity.

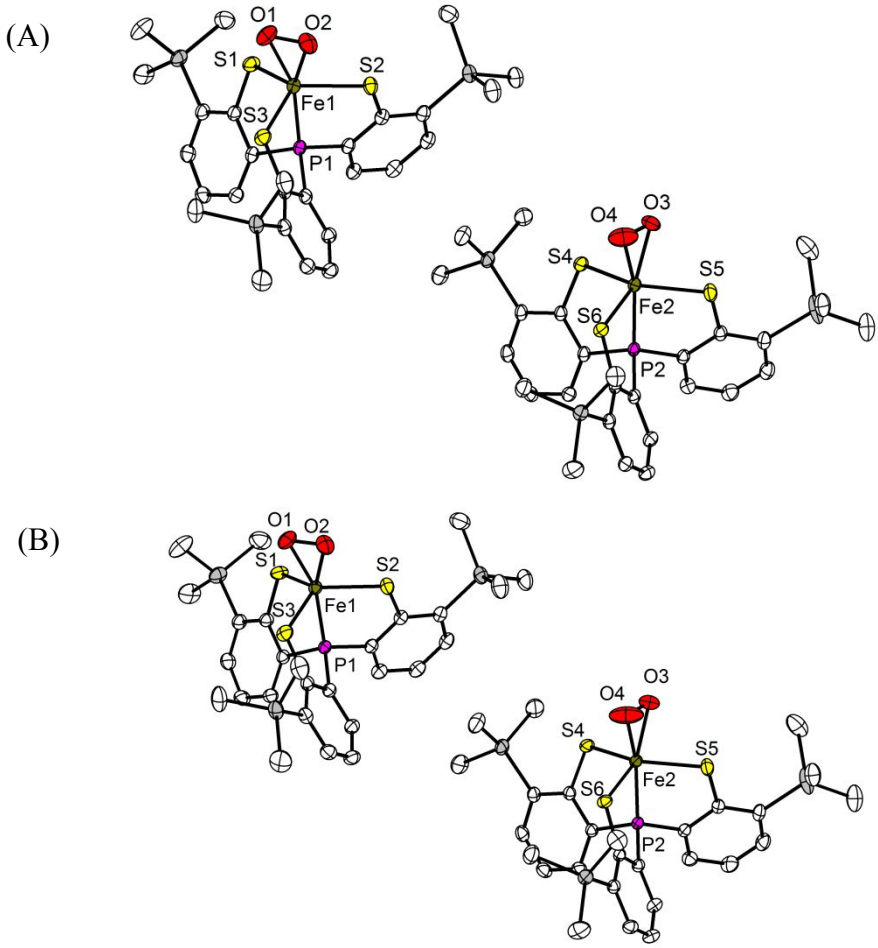

Figure S2. ORTEP diagrams of $[PPh_4][\mathbf{1}]\cdot 2THF$ collected at (A) 150 K and (B) 200 K. The cations, solvated THF and hydrogen atoms are omitted for clarity.

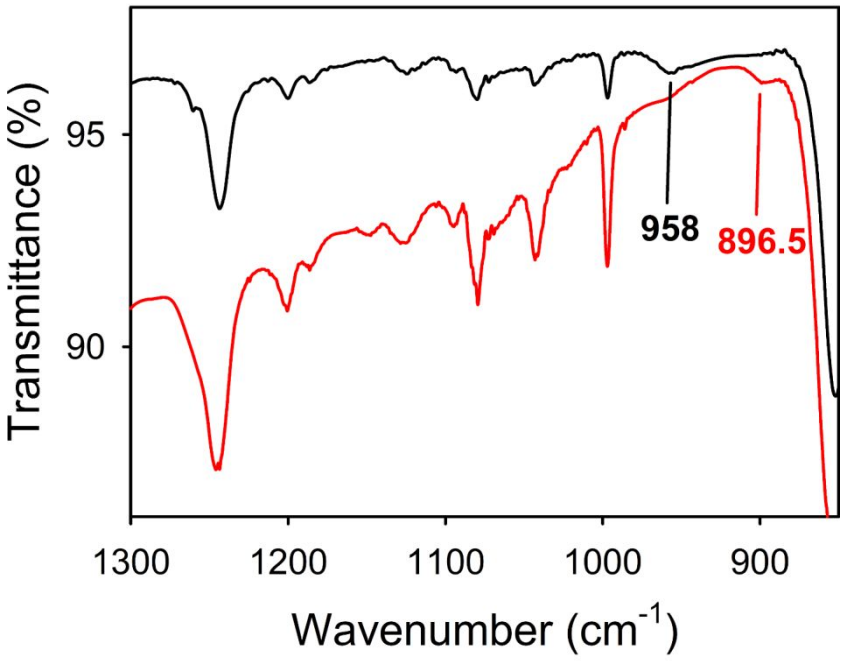

Figure S3. IR spectra of **1** in THF. **1-**$^{16}O_2$ (Black) and **1-**$^{18}O_2$ (red).

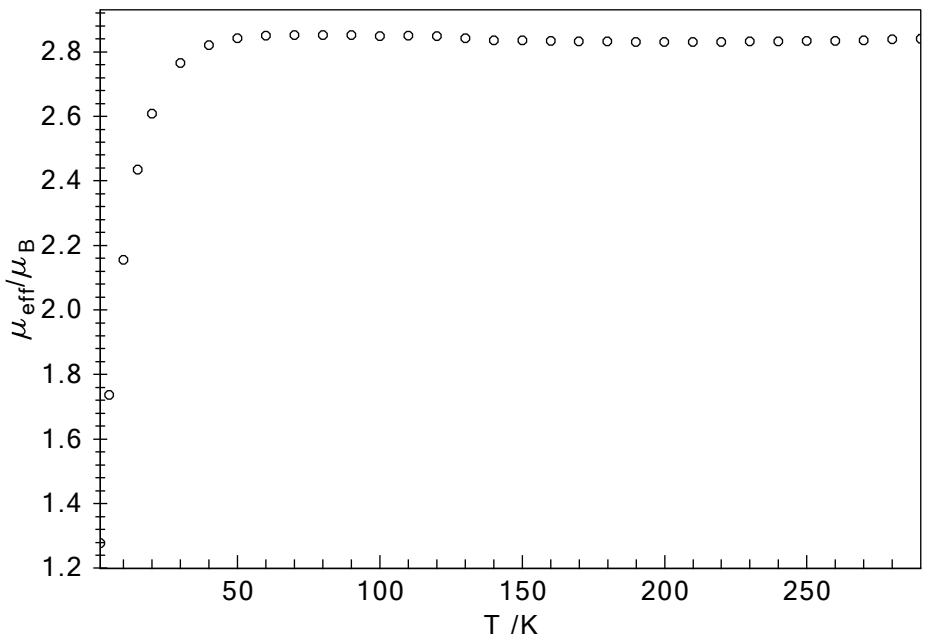

Figure S4. The measured effective magnetic moment of [$AsPh_4$][**1**] as a function of temperature.

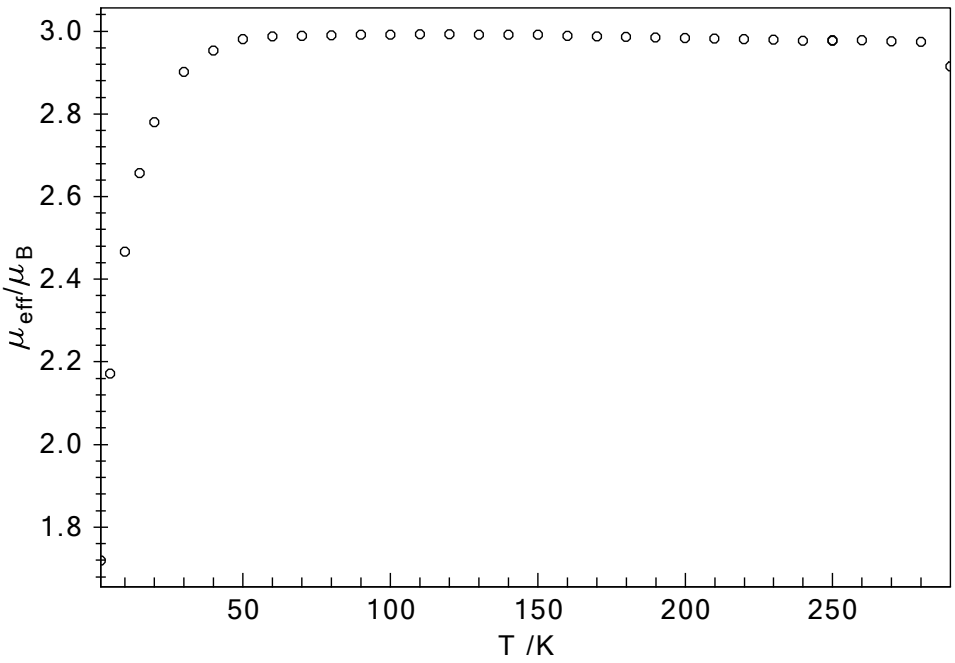

Figure S5. The measured effective magnetic moment of [PPh_4][**1**] as a function of temperature.

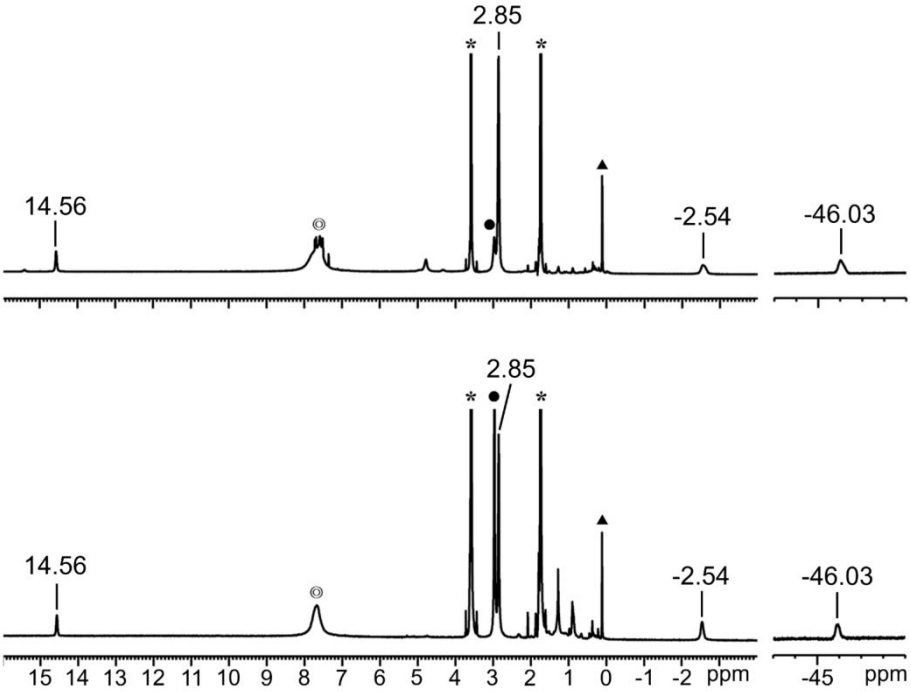

Figure S6. ^{1}H NMR spectra of [PPh_4][**1**] (top) and [$AsPh_4$][**1**] (bottom) in d_8-THF. The data were taken at 223 K. The peaks at 14.56, -2.54, -46.03 and 2.85 ppm are associated with H atoms of phenyl groups and trimethylsilyl groups in PS3". The peaks at 7~8 ppm are associated with H atoms of cations. *THF, ▲ contaminated grease, ● degradation product.

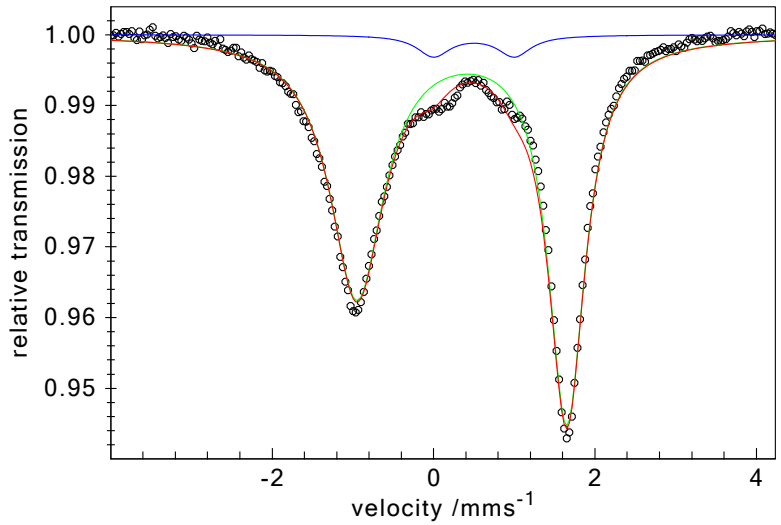

Figure S7. The Mössbauer spectrum of $[Fe^{III}(PS3'')(OCH_3)]^-$. Simulations give δ = 0.35 mm/s, ΔE_Q = 2.60 mm/s for 95% $[Fe^{III}(PS3'')(OCH_3)]^-$, and δ = 0.50 mm/s, ΔE_Q = 1.00 mm/s for 5% impurity.[a]

[a] Half-integer spin systems usually do not relax very fast even at low temperatures, and are in the so-called intermediate relaxation regime; consequently, their Mössbauer spectra often show asymmetric broadening as exemplified by that of $[Fe^{III}(PS3'')(OCH_3)]^-$ (Figure 3). Increasing temperatures speeds up relaxation and often leads to well-resolved quadrupole doublets as typically found for diamagnetic or integer spin systems. For $[Fe^{III}(PS3'')Cl]^-$, our initial attempt at 80 K gave a very broad spectrum, so the Mössbauer measurements were carried out at a higher temperature. Despite remaining slightly asymmetric, the 273 K spectrum has a much higher resolution, which enabled us to precisely abstract the Mössbauer parameters.

Due to the existence of the second-order Doppler shift, the isomer shift measured at higher temperatures may slightly lower than that at lower temperatures, but the difference, which depends on the Debye temperature of a given sample, is hardly greater than 0.1 mm/s. In the present case, even adding 0.1 mm/s to the isomer shift (0.33 mm/s) determined at 273 K does not affect the correctness of the conclusion.

Indeed, the sample of $[Fe^{III}(PS3'')(OCH_3)]^-$ contains some impurity; however, after repeated attempts of simulations, we found that the Fe content of the impurity is no more than 5%, a typical spectrum shown below.

Computational detail

The B3LYP density functional was used to compute the spin-state energetics and tested the following initial guesses for the electronic structure of complex **1**, namely, (a) BS(6,0) describing a high spin ferric center ferromagnetically coupled to a superoxo radical; (b) BS(4,0) describing an intermediate spin ferric center ferromagnetically coupled to a superoxo radical; (c) BS(5,1) describing a high spin ferric center antiferromagnetically coupled to a superoxo radical; (d) BS(3,1) describing an intermediate spin ferric center antiferromagnetically coupled to a superoxo radical; (e) BS(2,0) describing a low spin ferric center ferromagnetically coupled to a superoxo radical or an intermediate spin Fe^{IV} center bound to a peroxo ligand. Our theoretical results demonstrated that the BS(2,0) calculations invariably converged to the BS(3,1) solution, and that the BS(6,0), BS(4,0) and BS(5,1) states lie 22.0, 13.4, and 18.9 kcal/mol higher in energy above BS(3,1). Thus, the DFT calculations unambiguously predicts BS(3,1) to be the ground state, consistent with the spin density plot and important atomic spin populations (Figure 4C). More importantly, our CASSCF(20,14) computation further confirmed the electronic structure deduced by DFT calculations (Figure 4A).

However, B3LYP geometry optimizations without any constraints erroneously predicted that the end-on isomer of **1** is stabilized by 9.4 kcal/mol relative to the side-on isomer; consequently, when the O-O bond distances is shorter than 1.27 Å in the relaxed surface scan, the calculations always delivered a geometry with an end-on O_2 ligand. While PBE computations suggest the end-on isomer to be 4.8 kcal/mol above the side-on isomer, and the PBE relaxed surface scan retained an O_2 side-on coordination geometry irrespective of the O-O bond length. More importantly, the PBE computed Mössbauer parameters and O-O stretching frequencies of the BS(3,1) solution are all in reasonable agreement with the experiment within the uncertainty range of the computations (Table S11). Thus, PBE is employed for the relaxed surface scan.

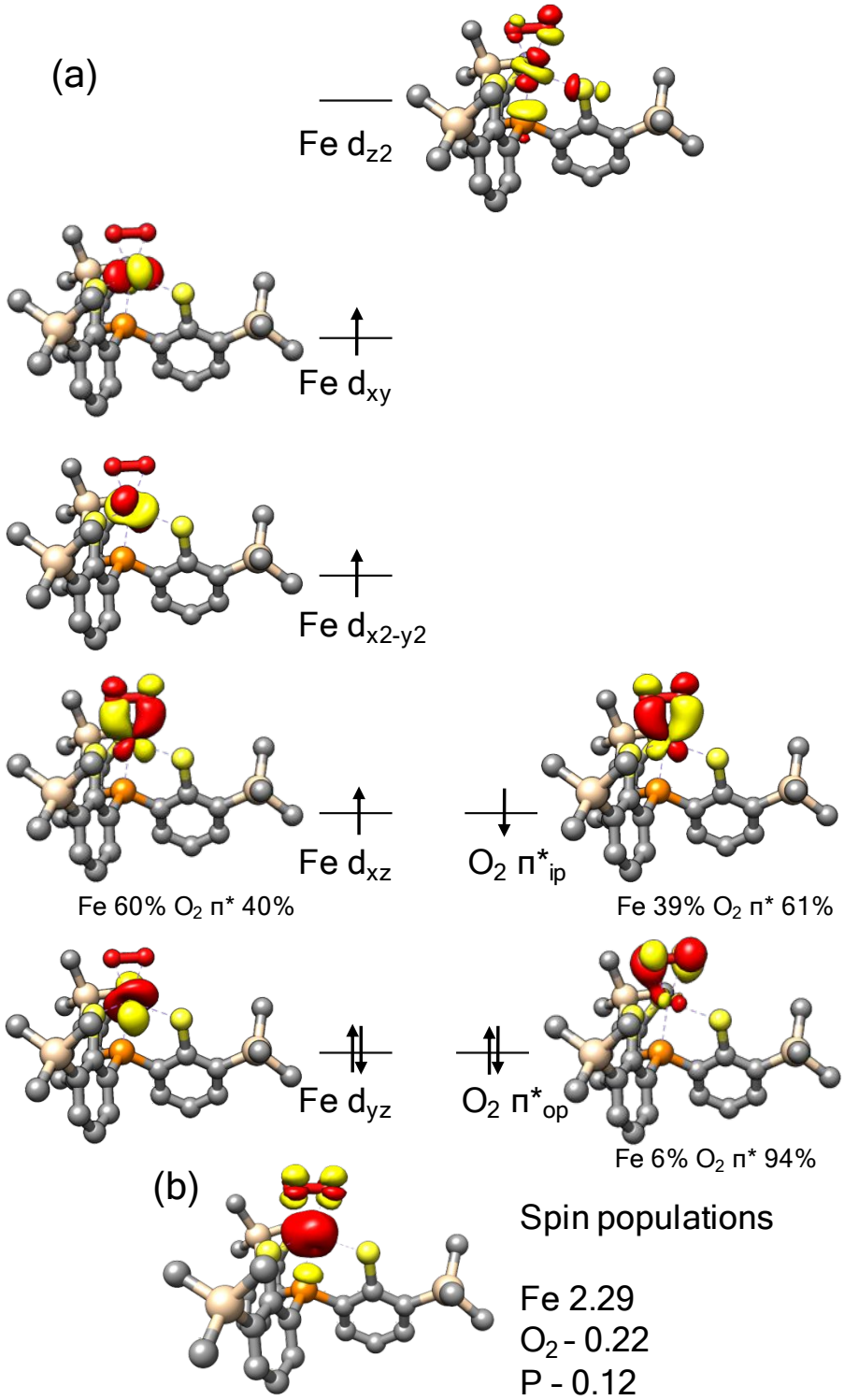

Figure S8. (a) molecular orbital diagram of complex **1** constructed by using B3LYP unrestricted corresponding orbitals. (b) spin density plot and important atomic spin populations.

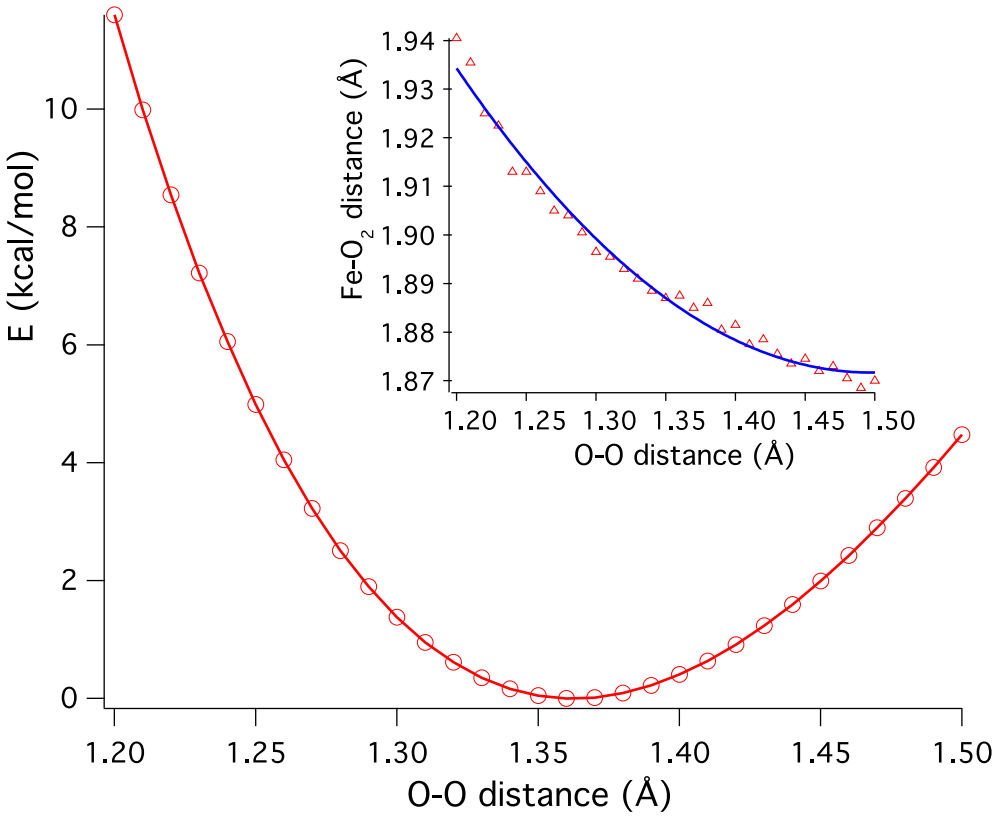

Figure S9. The PBE computed energy change and the average Fe-O_2 bond length (inset) of **1** as a function of the O-O bond distance.

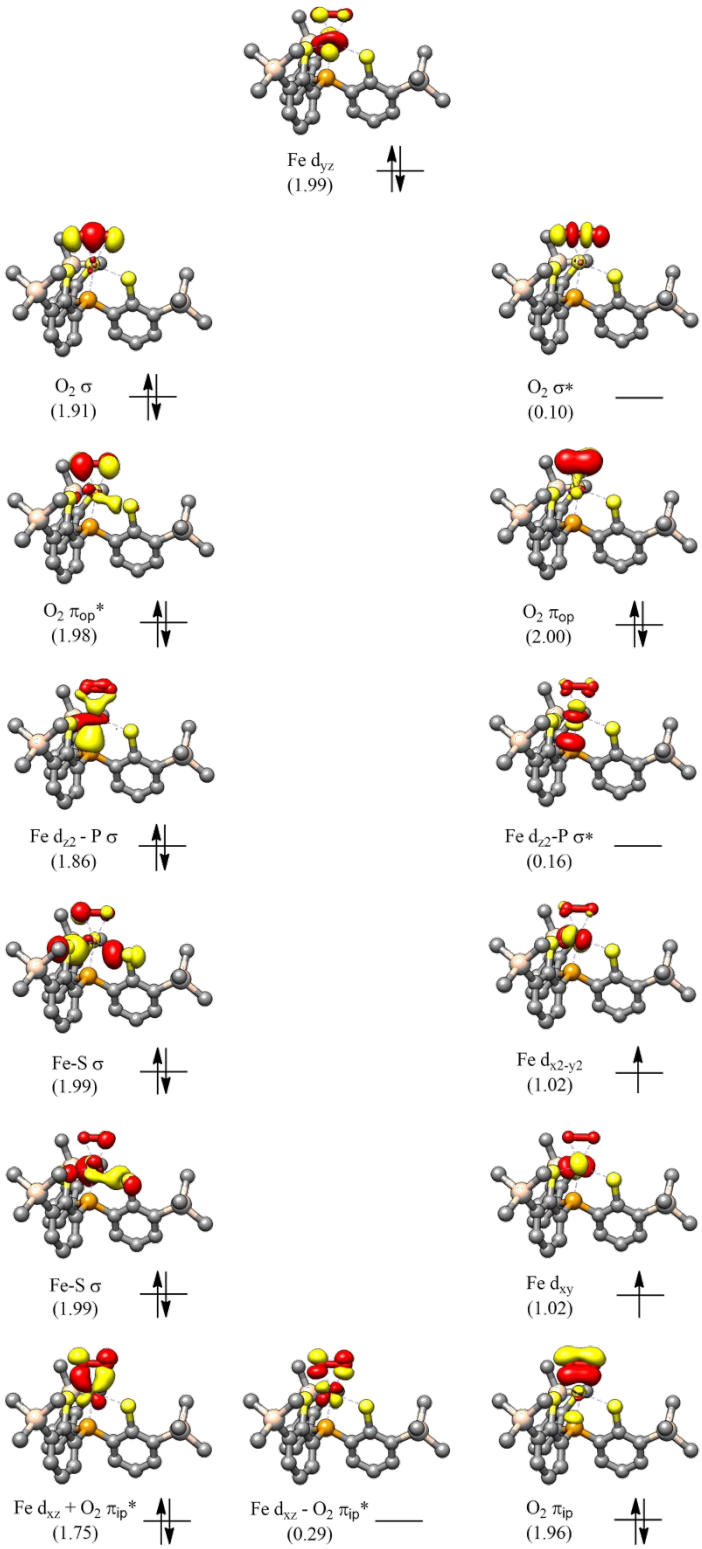

Figure S10. Electronic structure of complex **1** with an O-O bond distance of 1.50 Å derived from CASSCF(20,14) calculations. Natural orbitals with occupation number in parentheses.

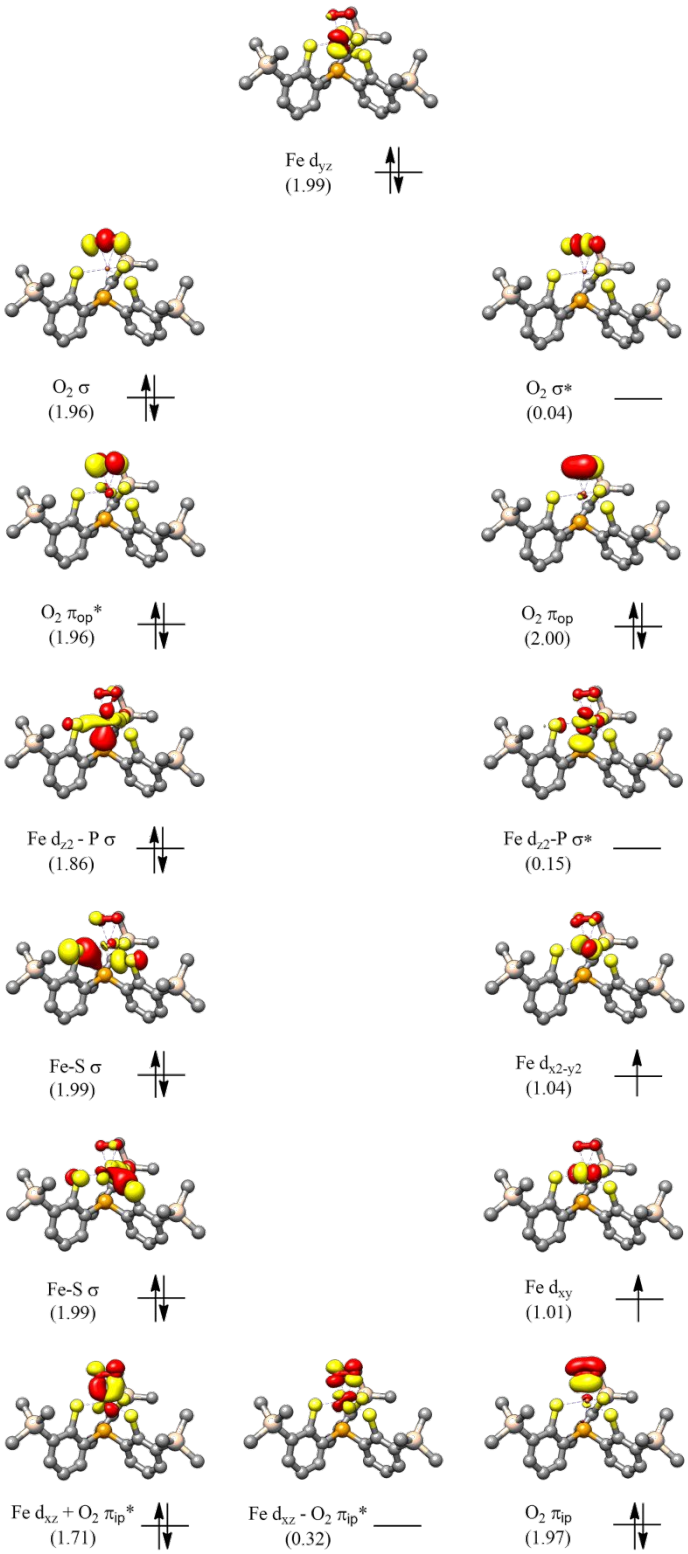

Figure S11. Electronic structure of complex **1** with an O-O bond distance of 1.23 Å derived from CASSCF(20,14) calculations. Natural orbitals with occupation number in parentheses.

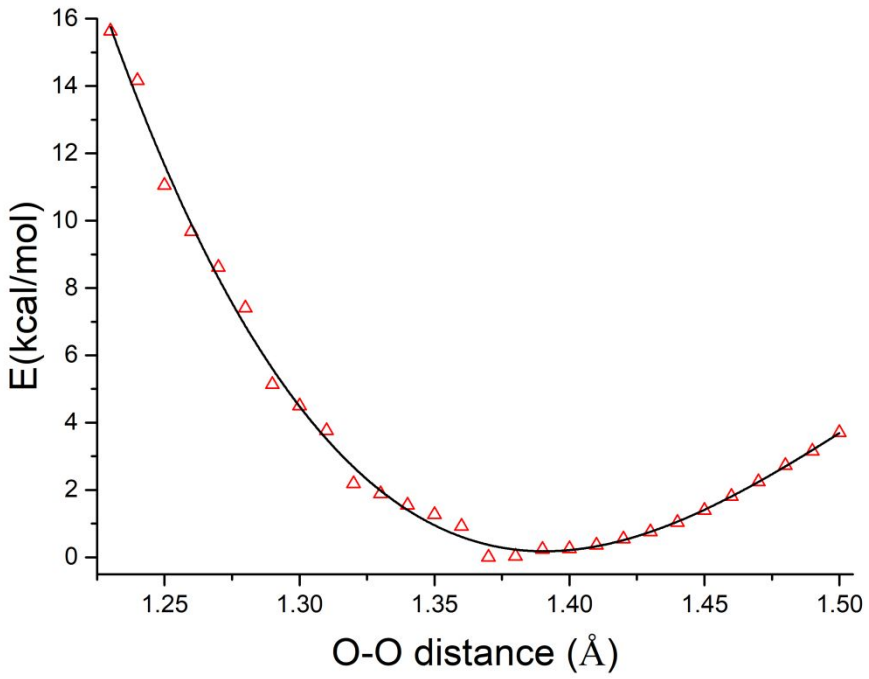

Figure S12. The CASSCF(20,14) computed energy change of **1** as a function of the O-O bond distance.

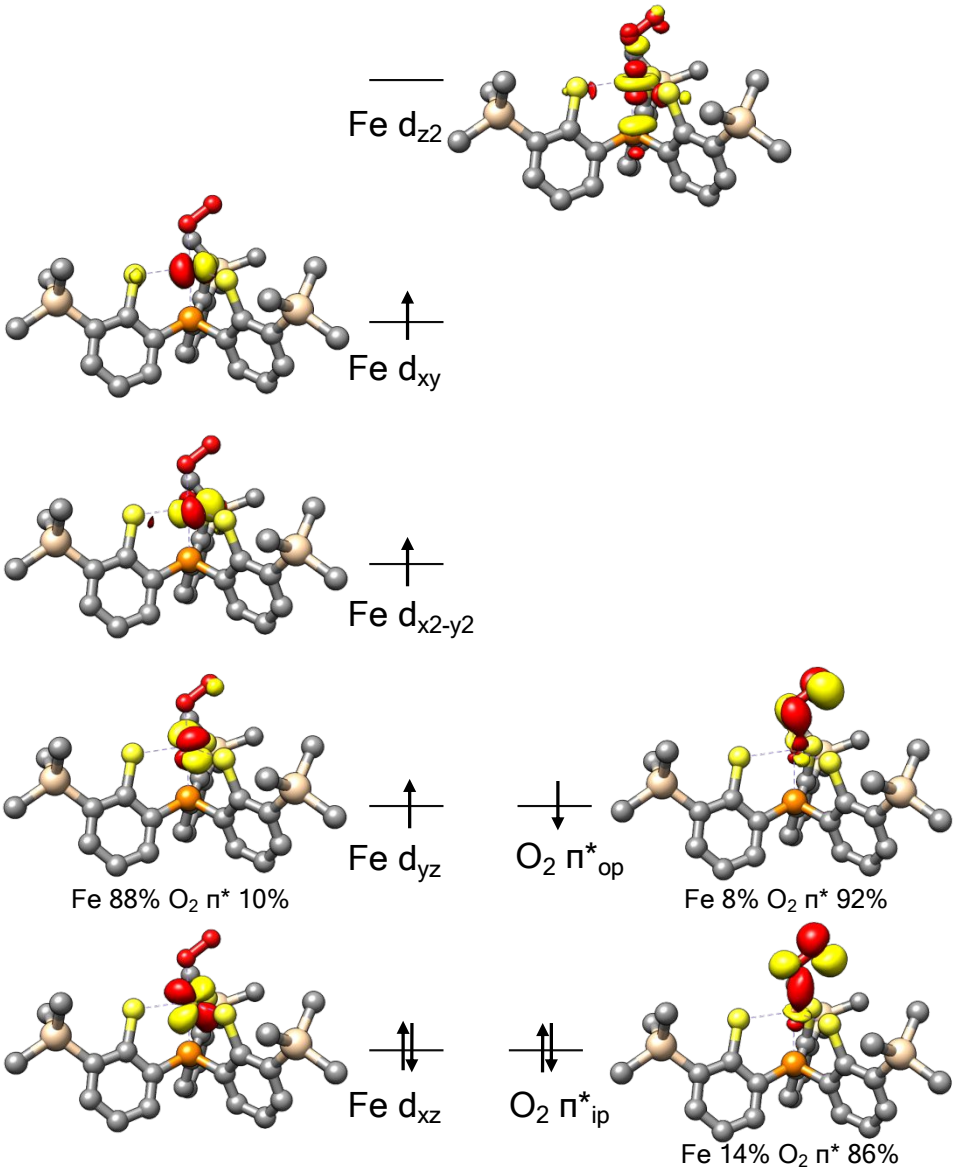

Figure S13. MO diagram of the end-on O_2 isomer of **1** obtained by B3LYP calculations.

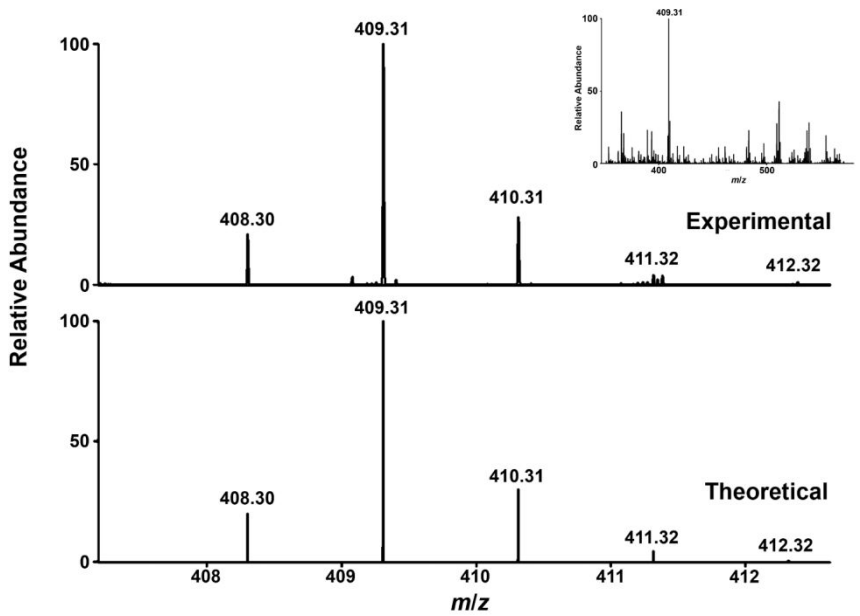

Figure S14. The ESI-MS spectrum (negative mode) of the post-reaction solution of **1** and 2,6-di-*tert*-butylphenol at -20 °C. The experimental data is consistent with the calculated one composed of 10% [$C_{28}H_{40}O_2$] and 90% [$C_{28}H_{41}O_2$]. ([$C_{28}H_{40}O_2$] and [$C_{28}H_{41}O_2$] are assigned to 3,3',5,5'-tetra-tert-butyl-4,4'-diphenoquinone and a deprotonated form of 4,4'-dihydroxy-3,3',5,5'-tetra-tert-butyl-diphenyl, respectively.) Inset: the spectrum in the full range.

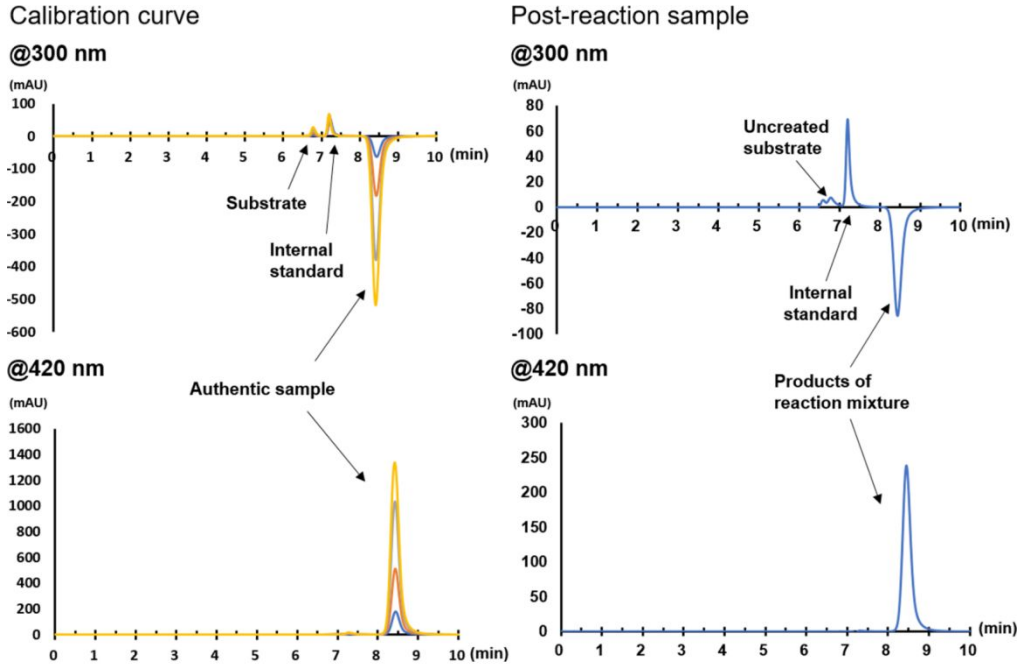

Figure S15. LC analysis for the reaction of **1** with 2,6-di-*tert*-butylphenol at -20 °C. Left: Determination of calibration curve by using benzil as an internal standard (detected at 300 nm) and 4,4'-dihydroxy-3,3',5,5'-tetra-tert-butyl-diphenyl as an authentic sample (detected at 420 nm). Right: Determination of products for the post-reaction sample.

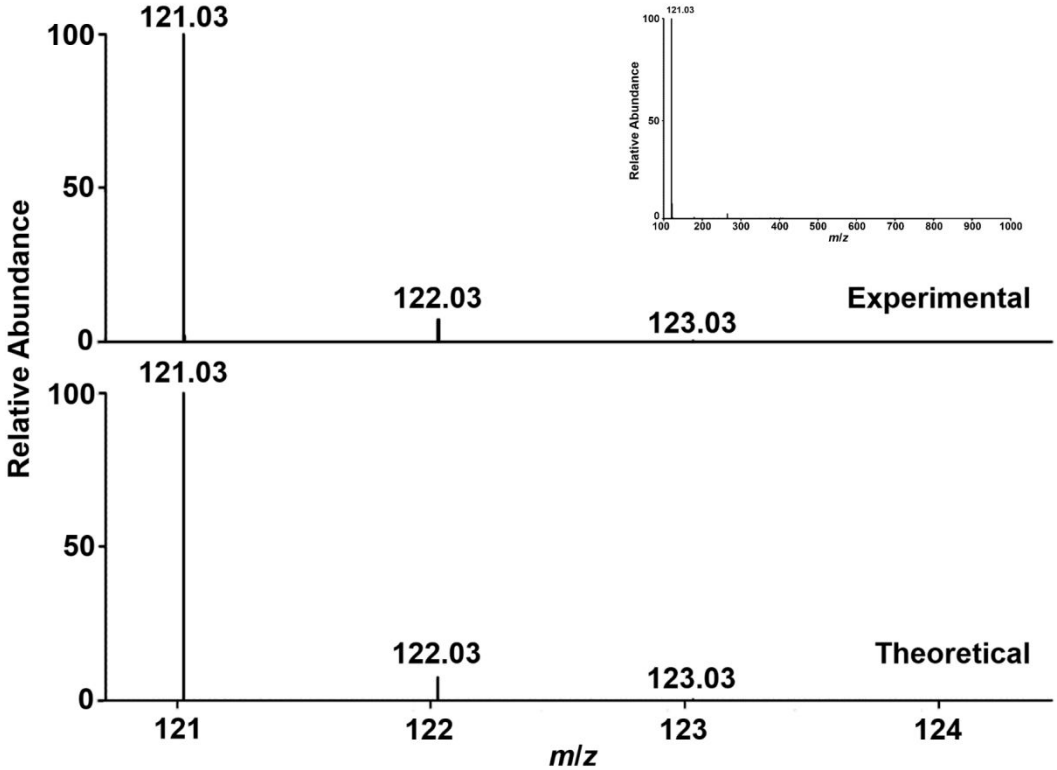

Figure S16. The ESI-MS spectrum (negative mode) of the post-reaction solution of **1** and benzaldehyde at -20 °C. The experimental data is consistent with the calculated one of $[C_7H_5O_2]$. ($[C_7H_5O_2]$ is assigned to benzoate.) Inset: the spectrum in the full range.

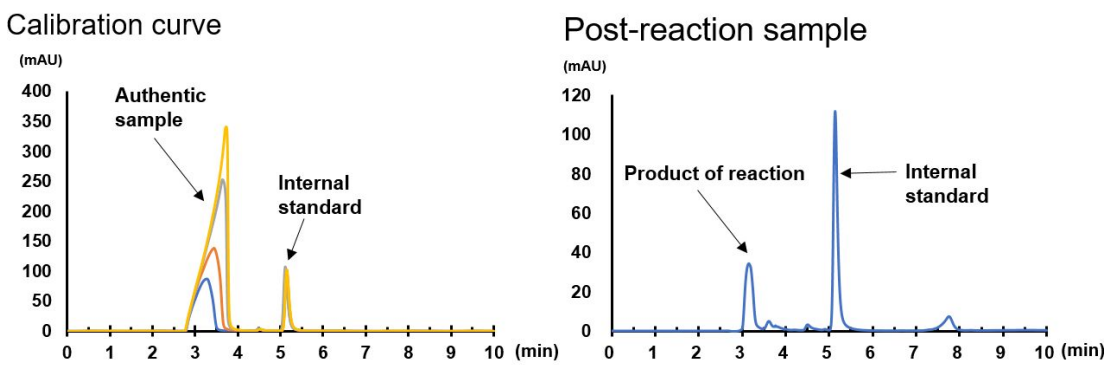

Figure S17. LC analysis for the reaction of **1** with benzaldehyde at -20 °C. Left: Determination of calibration curve by using phenol as an internal standard and benzoic acid as an authentic sample (detected at 230 nm). Right: Determination of products for the post-reaction sample.

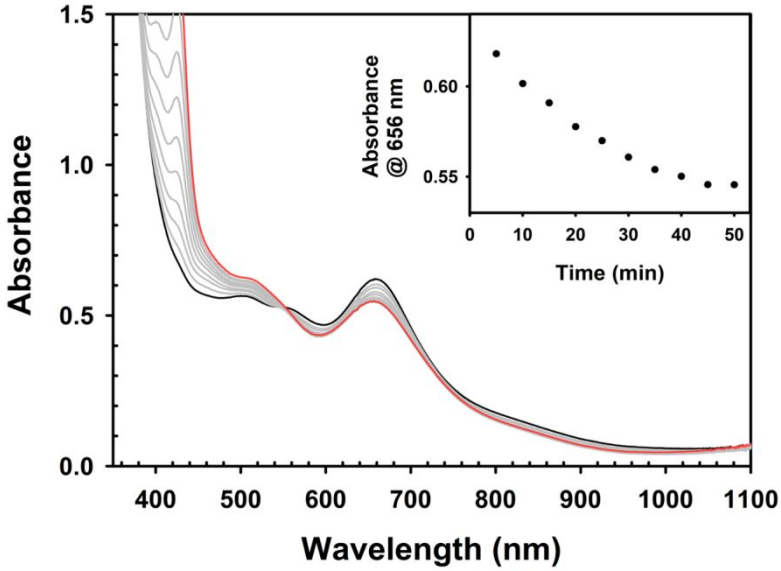

Figure S18. UV-vis-NIR spectral change of **1** (0.2 mM) reacting with 2,6-di-*tert*-butylphenol (0.32 M) in THF at -20 °C (from black to red). Inset: The absorbance at 656 nm decays against time.

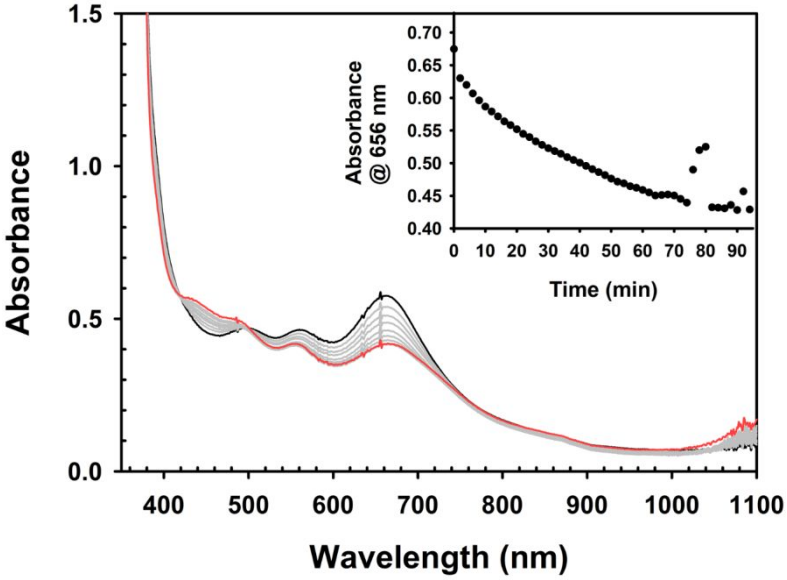

Figure S19. UV-vis-NIR spectral change of **1** (0.2 mM) reacting with benzaldehyde (0.15 M) in THF at -20 °C (from black to red). Inset: The absorbance at 656 nm decay against time.

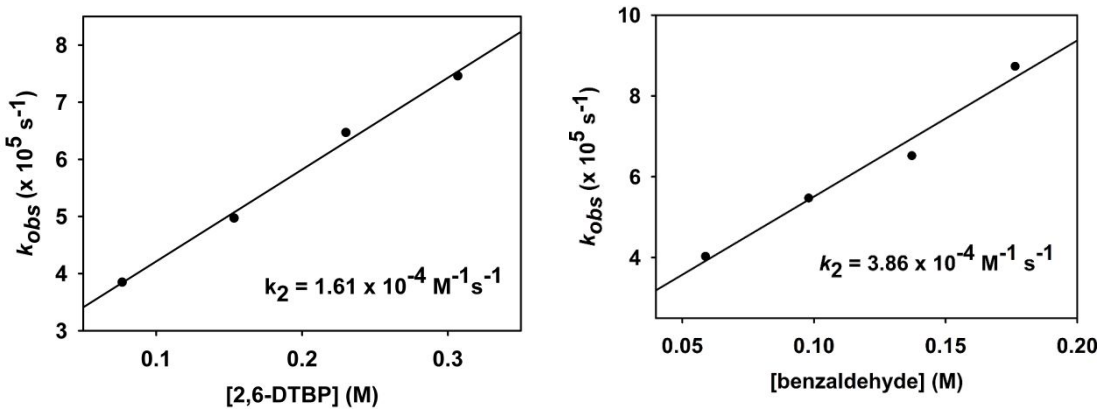

Figure S20. Second-order rate constant k_2
obtained from the reaction of **1** and substrates at -20 °C. The k_2 values derivate from pseudo-first order rate constant k_{obs} (s^{-1}) versus concentration (M) of 2,6-di-*tert*-butylphenol (left) and benzaldehyde (right).

Table S1. The O-O bond distances in the reported examples of the first-row *d*-block metal-superoxo complexes.

Reference	Complex	Bond length of O-O (Å)
1	$[Fe(TAML)(O_2)]^{2-}$	1.323(3), 1.306(7)
2	$[Cr(14\text{-}TMC)(O_2)(Cl)]^{+}$	1.231(6)
3	$[Tp'Co(O_2)]$	1.355(3)
4	$[Tp^{tBu,Me}Cr(pz'H)(O_2)]^{+}$	1.327(5)
5	$[LNi(O_2)]$	1.347(2)
6	$[Co(L^{OiPr})(Tp^{Me2})(O_2)]$	1.301(5)
7	$[Cu(TMG_3tren)(O_2)]^{+}$	1.280
8	$[(^{Ar}L)Cu(O_2)]$	1.383(2)
This work	$[PPh_4]$[**1**]	1.330(4), 1.229(4)
		1.340(3), 1.221(4)
		1.351(3), 1.207(4)
	$[AsPh_4]$[**1**]	1.387(2)

Table S2. The O-O bond distances in the reported examples of the first-row *d*-block metal-peroxo complexes.

Reference	Complex	Bond length of O-O (Å)
9	$[CrO_2(tpenaH)]^{2+}$	1.383(8)
10	$[Cr(12\text{-}TMC)(O_2)(OH_2)]^{2+}$	1.394(4)
11	$[Cr(dien)(O_2)_2]$	1.465(2), 1.456(2)
12		1.465(2)
13	$[Mn(14\text{-}TMC)(O_2)]^{+}$	1.410(4)
14	$[Mn(O_2)(P(C_6H_3\text{-}3\text{-}SiMe_3\text{-}2\text{-}S)_3)]^{-}$	1.379(3)
15	$[Tp^{iPr2}Mn(\eta^2\text{-}O_2)(im^{Me}H)]$	1.42(1)
16	$[MnTPPO_2]^{-}$	1.421(5)
17	$[Mn(12\text{-}TMC)(O_2)]^{+}$	1.408(avg)
18	$[Mn(tmc)(O_2)]^{+}$	1.403(4)
19	$[Mn(O_2)(Tp^{iPr2})(pz^{iPr2}H)]$	1.432(3)
20	$[Mn(O_2)(3,5\text{-}iPr_2pzH)(HB(3,5\text{-}iPr_2pz)_3)]$	1.428(7), 1.43(1)
1	$[Mn(TAML)(O_2)]^{2-}$	1.415(2), 1.412(3)
21	$[Fe(TMC)(OO)]^{+}$	1.463(6)
22	$[NiLFe(\eta^2\text{-}O_2)(\eta^5\text{-}C_5Me_5)]^{+}$	1.381(3)
23	$[Co(tmen)_2O_2]^{+}$	1.457(3)
24	$(+)_{546}$-Δ-*cis*-β-[Co{R,R-$(CH_3)_2As(CH_2)_3As(C_6H_5)(CH_2)_2As(C_6H_5)(CH_2)_3As(CH_3)_2$}$O_2$]	1.424(10)
25	$[O_2Co(2{=}phos)_2]^{+}$	1.420(10)
26	$[Co_2(CN)_4(PMe_2Ph)_5(O_2)]$	1.441(11)
27	$[(TIMEN^{xyl})Co(O_2)]^{-}$	1.429(3)
28	$[L^{tBu}Co(O_2)]$	1.361(5)
29	$[Co(12\text{-}TMC)(O_2)]^{+}$	1.4389(17)
	$[Co(13\text{-}TMC)(O_2)]^{+}$	1.438(4)
30	[Co(3-*t*-Bu-Salen)·O2]	1.350(11)
31	$[Co(bbpc)(O2)]^{+}$	1.4484(42), 1.4319(60)
32	$[Co(TBDAP)(O_2)]^{+}$	1.456(3)
33	$[Ni(TBDAP)(O_2)]^{+}$	1.401(2)
34	$[Ni(13\text{-}TMC)(O_2)]^{+}$	1.383(4)
35	$[Ni(12\text{-}TMC)(O_2)]^{+}$	1.386(4)
36	L^2CuO_2	1.392(12)
37		1.44(2)
38	L^2CuO_2	1.392(3)

Table S3. Crystallographic data of $[AsPh_4][Fe(PS3'')(CH_3CN)]\cdot 5CH_3CN$

	$[AsPh_4][Fe(PS3'')(CH_3CN)]\cdot 5CH_3CN$
Chemical formula	$C_{63}H_{74}AsFeN_6PS_3Si_3$
Fw	1257.47
T, K	200(2)
Crystal system	Triclinic
Space group	$P\bar{1}$
a, Å	14.6564(3)
b, Å	14.9077(3)
c, Å	17.3142(3)
α, deg	101.6193(7)
β, deg	99.9232(6)
γ, deg	111.9234(7)
V, Å^3	3307.5 (1)
Z	2
D_{cala}/g cm^{-3}	1.263
GOF[a] on F^2	1.031
R_1, [b]%	0.0460
wR_2, [c]%	0.1230
CCDC number	2019735

[a]GOF=$\{\Sigma[w(F_o^2-F_c^2)^2]/(M-N)\}1/2$($M$=number of reflections, N=number of parameters refined)

[b]$R1 = \Sigma||F_o| - |F_c||/\Sigma||F_o|$.

[c]$wR2 = \{\Sigma[w(F_o^2 - F_c^2)^2]/\Sigma[w(F_o^2)^2]\}^{1/2}$.

Table S4. Selected bond distances (Å) and bond angles (deg) of $[AsPh_4][Fe(PS3")(CH_3CN)]\cdot 5CH_3CN$

Bond length (Å)		Bond angle (degree)	
Fe-S(1)	2.2831(8)	S(1)-Fe-S(2)	122.79(3)
Fe-S(2)	2.2739(8)	S(2)-Fe-S(3)	119.24(3)
Fe-S(3)	2.2832(7)	S(1)-Fe-S(3)	117.11(3)
Fe-P(1)	2.1252(7)	S(1)-Fe-N(1)	95.07(7)
Fe-N(1)	1.962(2)	S(2)-Fe-N(1)	90.82(7)
		S(3)-Fe-N(1)	93.38(7)
		S(1)-Fe-P(1)	86.89(3)
		S(2)-Fe-P(1)	86.68(3)
		S(3)-Fe-P(1)	87.23(3)
		P(1)-Fe-N(1)	177.40(8)

Table S5. Crystallographic data of $[PPh_4][Fe(PS3'')(O_2)]\cdot 2THF$ ($[PPh_4][\mathbf{1}]\cdot 2THF$)

	$[PPh_4][Fe(PS3'')(O_2)]\cdot 2THF$		
Chemical formula	$C_{59}H_{72}FeO_4P2S_3Si_3$		
Fw	1143.40		
Crystal system	Triclinic		
Space group	$P\bar{1}$		
T, K	100(2)	150(2)	200(2)
a, Å	14.5392(3)	14.5658(3)	14.5755(4)
b, Å	21.4172(5)	21.5165(5)	21.6461(6)
c, Å	22.4147(5)	22.4637(5)	22.5489(6)
α, deg	116.7215(5)	116.7625(5)	116.8398(6)
β, deg	92.1584(6)	92.2027(6)	92.2390(6)
γ, deg	106.3529(6)	106.2783(6)	106.1547(7)
V, Å^3	5871.2(2)	5921.7(2)	5983.6(3)
Z	4	4	4
D_{cala}/g cm^{-3}	1.294	1.283	1.269
GOF[a] on F^2	1.019	1.016	1.028
R_1, [b]%	0.0525	0.0462	0.0484
wR_2, [c]%	0.1363	0.1199	0.1261
CCDC number	1957950	1957951	1957952

[a]GOF=$\{\Sigma[w(F_o^2-F_c^2)^2]/(M-N)\}1/2$ (M=number of reflections, N=number of parameters refined)

[b]$R_1 = \Sigma||F_o| - |F_c||/\Sigma||F_o|$.

[c]$wR_2 = \{\Sigma[w(F_o^2 - F_c^2)^2]/\Sigma[w(F_o^2)^2]\}^{1/2}$.

Table S6. Crystallographic data of $[AsPh_4][Fe(PS3")(O_2)]\cdot 2THF$ ($[AsPh_4]$[**1**]$\cdot$2THF)

	$[AsPh_4][Fe(PS3")(O_2)]\cdot 2THF$
Chemical formula	$C_{59}H_{72}FeO_4P2S_3Si_3$
Fw	1187.35
Crystal system	Triclinic
Space group	$P\bar{1}$
T, K	100(2)
a, Å	11.3019(3)
b, Å	14.6788(4)
c, Å	19.2169(6)
α, deg	95.9416(6)
β, deg	97.0774(5)
γ, deg	108.1750(5)
V, Å^3	2971.7(2)
Z	2
D_{cala}/g cm^{-3}	1.327
GOF[a] on F^2	1.051
R_1, [b]%	0.0334
wR_2, [c]%	0.0892
CCDC number	1957946

[a]GOF=$\{\Sigma[w(F_o^2-F_c^2)^2]/(M-N)\}1/2$ (M=number of reflections, N=number of parameters refined)

[b]$R_1 = \Sigma||F_o| - |F_c||/\Sigma||F_o|$.

[c]$wR_2 = \{\Sigma[w(F_o^2 - F_c^2)^2]/\Sigma[w(F_o^2)^2]\}^{1/2}$.

Table S7. Selected bond distances (Å) and bond angles (deg) of $[PPh_4][Fe(PS3")(O_2)]\cdot 2THF$ ($[PPh_4][\mathbf{1}]\cdot 2THF$)

Temperature (K)	100	150	200
Bond length (Å)			
Fe(1)-O(1)	1.888(3)	1.894(2)	1.893(2)
Fe(1)-O(2)	1.880(2)	1.890(2)	1.890(2)
O(1)-O(2)	1.330(4)	1.340(3)	1.351(3)
Fe(1)-P(1)	2.2036(8)	2.2030(7)	2.2038(6)
Fe(1)-S(1)	2.3417(8)	2.3287(7)	2.3225(6)
Fe(1)-S(2)	2.3164(8)	2.3089(7)	2.3047(6)
Fe(1)-S(3)	2.3247(8)	2.3202(7)	2.3154(7)
Fe(2)-O(3)	1.942(3)	1.941(2)	1.928(2)
Fe(2)-O(4)	1.890(3)	1.892(2)	1.875(2)
O(3)-O(4)	1.229(4)	1.221(4)	1.207(4)
Fe(2)-P(2)	2.2142(8)	2.2129(6)	2.2126(6)
Fe(2)-S(4)	2.2995(7)	2.2953(6)	2.2919(6)
Fe(2)-S(5)	2.3029(8)	2.2941(7)	2.2902(6)
Fe(2)-S(6)	2.3275(8)	2.3266(7)	2.3238(6)
Bond angle (degree)			
O(1)-Fe(1)-O(2)	41.3 (1)	41.5(1)	41.84(9)
Fe(1)-O(1)-O(2)	69.0(2)	61.1(1)	69.0(1)
Fe(1)-O(2)-O(1)	69.7(2)	69.4(1)	69.2(1)
P(1)-Fe(1)-S(1)	80.36(3)	80.62(2)	80.71(2)
P(1)-Fe(1)-S(2)	80.46(3)	80.50(2)	80.54(2)
P(1)-Fe(1)-S(3)	80.66(3)	80.53(2)	80.43(2)
S(1)-Fe(1)-S(2)	114.36(3)	114.45(3)	114.54(3)
S(2)-Fe(1)-S(3)	119.07(3)	119.19(3)	119.27(3)
S(1)-Fe(1)-S(3)	118.55(3)	118.43(3)	118.26(3)
O(3)-Fe(2)-O(4)	37.4 (1)	37.1(1)	37.0(1)
Fe(2)-O(3)-O(4)	69.0(2)	69.3(1)	69.1(1)
Fe(2)-O(4)-O(3)	73.6(2)	73.6(2)	73.9(2)
P(2)-Fe(2)-S(4)	83.33(3)	83.73(2)	83.61(2)
P(2)-Fe(2)-S(5)	80.58(3)	80.83(2)	80.90(2)
P(2)-Fe(2)-S(6)	81.54(3)	81.48(2)	81.43(2)
S(4)-Fe(2)-S(5)	127.50(3)	127.07(3)	126.67(3)
S(5)-Fe(2)-S(6)	118.06(3)	118.23(3)	117.97(3)
S(4)-Fe(2)-S(6)	108.56(3)	108.88(2)	109.52(2)

Table S8. Selected bond distances (Å) and bond angles (deg) of $[AsPh_4][Fe(PS3")(O_2)]\cdot 2THF$ ($[AsPh_4][\mathbf{1}]\cdot 2THF$)

Bond length (Å)		Bond angle (degree)	
Fe-O(1)	1.884(1)	O(1)-Fe-O(2)	43.18(7)
Fe-O(2)	1.886(1)	Fe-O(1)-O(2)	68.48(8)
O(1)-O(2)	1.387(2)	Fe-O(2)-O(1)	68.34(8)
Fe-P(1)	2.2054(5)	P(1)-Fe(1)-S(1)	79.57 (2)
Fe-S(1)	2.3171(5)	P(1)-Fe(1)-S(2)	81.63(2)
Fe-S(2)	2.3171(5)	P(1)-Fe(1)-S(3)	80.61(2)
Fe-S(3)	2.2930(5)	S(1)-Fe(1)-S(2)	112.28 (2)
		S(2)-Fe(1)-S(3)	116.95(2)
		S(1)-Fe(1)-S(3)	122.85(2)

Table S9. The equivalent isotropic displacement parameters of O atoms of $[PPh_4][\mathbf{1}]\cdot 2THF$ and $[AsPh_4][\mathbf{1}]\cdot 2THF$

Compound	Temperature (K)	U_{eq} ($Å^2$x 10^3)			
		O1	O2	O3	O4
$[PPh_4][\mathbf{1}]\cdot 2THF$	100	54(1)	48(1)	61(1)	62(1)
	150	50(1)	48(1)	64(1)	70(1)
	200	51(1)	50(1)	73(1)	89(1)
$[AsPh_4][\mathbf{1}]\cdot 2THF$	100	29(1)	28(1)	-	-

Table S10. The O-O vibrational energy in the reported examples of the first-row *d*-block metal-superoxo complexes.

Reference	Complex	Wavenumber (cm^{-1})	
		$\nu_{16O-16O}$	$\nu_{18O-18O}$
1	$[Fe(TAML)(O_2)]^{2-}$	1260	1183
2	$[Cr(14\text{-}TMC)(O_2)(Cl)]^{+}$	1170	1104
4	$[Tp^{tBu,Me}Cr(Ph)(O_2)]$	1027	969
	$[Tp^{tBu,Me}Cr(OPh)(O_2)]$	1068	1009
	$[Tp^{tBu,Me}Cr(pz'H)(O_2)]^{+}$	1072	1007
	$[Tp^{tBu,Me}Cr(py)(O_2)]^{+}$	1083	1025
	$[Tp^{tBu,Me}Cr(Cl)(O_2)]$	1104	1044
5	$[LNi(O_2)]$	971	919
6	$[Co(L^{OiPr})(Tp^{Me2})(O_2)]$	1147	1088
	$[Co(L^{Ph})(Tp^{Me2})(O_2)]$	1150	1090
	$[Fe(L^{Ph})(Tp^{Me2})(O_2)]$	1168	1090
7	$[Cu(TMG_3tren)(O_2)]^{+}$	1117	1059
34	$[Ni(13\text{-}TMC)(O_2)]^{+}$	1130	1070
39	$[Tp'Co(O_2)]$	961	908
40	$[Cu(O_2)(HB(3\text{-}^{t}Bu\text{-}5\text{-}^{i}Prpz)_3)]$	1112	1060
41	$[Ni(tmc)(O_2)]^{+}$	1131	1067
42	$[LNi(O_2)]^{-}$	980	932
43	$[Co(BDPP)(O_2)]$	1135	1070
44	$[Fe(BDPP)(O_2)]$	1125	1062
45	$[Mn(BDPP)(O_2)]$	1145,1125[a]	1073
	$[Mn(BDP^{Br}P)(O_2)]$	1145, 1125[a]	1078, 1064[a]
46	$[Co(Tp^{Me2})(CysOEt)(O_2)]$	1152	1091
47	$[Fe(Tp^{Me2})(2\text{-}ATP)(O_2)]$	1120	1055
48	$[Cu(NMe_2\text{-}TMPA)(O_2)]$	1121	1058
49	$[Cu(L^{H})(O_2)]^{-}$	1033	968
50	$[Fe(S_2^{Me2}N_3(Pr,Pr))(O_2)]$	1093, 1122[a]	1022
50	$[Co(O_2)(Me_3TACN)(S_2SiMe_2)]$	1133/1123[b]	1070/1059[b]
51	$[^{tBu,Tol}DHP]NiO_2$	1105	1045
52	$[(F_8)Fe\text{-}(O_2)]$	1178	1114
53	$[(^{TMG}N_3S)CuO_2]^{+}$	1105	1042
54	$[(P^{ImH})Fe(O_2)]$	1171	1110

55	$[(P^{Im})Fe(O_2)]$	1180	1124
56	$[(F_8)Fe(O_2)]$	1178	1114
57	$[(^6L)Fe(O_2)Fe\text{-}Cl]^+$	1176	1113
58	$[Fe(OPhP)(O_2)]$	1147	1088
59	$[\alpha_4Fe(COOMe)_4(O_2)]$	1104, 967	951, 911
60	$[(^{DMA}N_3S)Cu(O_2)]^+$	1117	1056
61	$[(DMM\text{-}tmpa)Cu(O_2)]^+$	1121	1058
62	$[(HIPT_3tren)Cu(O_2)]$	1095	1034
63	$[(TMPA)Cu(O_2)]^+$	1119	1058
	$[(BA)Cu(O_2)]^+$	1123	1059
	$[(F_5BA)Cu(O_2)]^+$	1126	1062
64	$[(MPPA)Cu(O_2)]^+$	1130	1067
65	$[(^{NH2}TMPA)Cu(O_2)]^+$	1123	1064, 1051
	$[(^{(NH2)2}TMPA)Cu(O_2)]^+$	1121	1061
	$[(^{PV2}TMPA)Cu(O_2)]^+$	1138, 1117	1055
	$[(^{(CH3)}TMPA)Cu(O_2)]^+$	1121	1064, 1049
66	$[LCu(O_2)]$	1104	1044
This work	$[AsPh_4][\mathbf{1}]$	958, 939[a]	896
	$[PPh_4][\mathbf{1}]$	959, 939[a]	897

[a] Fermi doublet. [b] Two conformers of Co-O_2 moiety are proposed.

Table S11. Comparison of the computed key geometric and spectroscopic parameters with experiment.

	Fe-O_2 (Å)	O-O (Å)	Fe-S (Å)	Fe-P (Å)	$\nu_{O\text{-}O}$ (cm^{-1})	δ (mm/s)	$\lvert\Delta E_Q\rvert$ (mm/s)
Exp.	1.884, 1.886	1.387	2.317, 2.317, 2.293	2.205	958, 939	0.37	2.00
PBE	1.867, 1.902	1.363	2.343, 2.298, 2.265	2.174	1017	0.27	2.01
B3LYP	1.884, 1.884	1.361	2.375, 2.358, 2.350	2.224	1049	0.35	2.26
Crystal structure		1.330				0.32	2.14

Crystal structure		1.229				0.38	1.72

Coordinate of the optimized geometry of complex **1** with O-O bond distance of 1.40 Å

Fe	0.078186000000	-0.269302000000	-0.060747000000
S	1.797432000000	1.224680000000	-0.351694000000
S	0.782898000000	-2.397617000000	-0.398368000000
S	-1.934062000000	0.840239000000	-0.495247000000
P	0.074636000000	-0.226774000000	-2.239372000000
Si	3.520020000000	4.046993000000	-1.162549000000
Si	2.561680000000	-5.153350000000	-1.308673000000
Si	-5.197584000000	1.261913000000	-1.392055000000
O	0.021875000000	0.265005000000	1.761702000000
O	-0.557354000000	-0.988905000000	1.533224000000
C	0.742979000000	1.337581000000	-2.857260000000
C	0.493134000000	1.882647000000	-4.123333000000
H	-0.239588000000	1.400250000000	-4.789945000000
C	1.165693000000	3.051174000000	-4.512720000000
H	0.976961000000	3.499958000000	-5.499722000000
C	2.075271000000	3.649875000000	-3.621703000000
H	2.593651000000	4.567873000000	-3.942377000000
C	2.331360000000	3.137407000000	-2.330902000000
C	1.636418000000	1.950882000000	-1.938659000000
C	2.596116000000	4.695667000000	0.358289000000
H	2.106370000000	3.856426000000	0.891275000000
H	1.808859000000	5.417774000000	0.058996000000
H	3.292649000000	5.206252000000	1.056538000000
C	4.253858000000	5.541395000000	-2.087694000000
H	3.467609000000	6.263984000000	-2.388926000000
H	4.808501000000	5.233187000000	-2.998002000000
H	4.965506000000	6.076519000000	-1.424280000000
C	4.958409000000	2.927228000000	-0.644059000000
H	5.645444000000	3.462307000000	0.045157000000
H	5.538588000000	2.600858000000	-1.531492000000
H	4.576426000000	2.021981000000	-0.132644000000
C	1.099202000000	-1.533394000000	-2.960589000000
C	1.576388000000	-1.568725000000	-4.279231000000
H	1.376289000000	-0.723189000000	-4.955895000000
C	2.323458000000	-2.675268000000	-4.711101000000
H	2.711021000000	-2.718190000000	-5.740221000000
C	2.582653000000	-3.725975000000	-3.810397000000

H	3.172195000000	-4.586496000000	-4.166223000000
C	2.135964000000	-3.711418000000	-2.471239000000
C	1.383305000000	-2.574918000000	-2.038806000000
C	3.629912000000	-4.559519000000	0.137725000000
H	3.094768000000	-3.777694000000	0.712516000000
H	4.578879000000	-4.122661000000	-0.234206000000
H	3.875299000000	-5.399907000000	0.820265000000
C	3.562166000000	-6.442762000000	-2.289436000000
H	3.813957000000	-7.298506000000	-1.628958000000
H	4.515257000000	-6.023568000000	-2.672338000000
H	2.989550000000	-6.840616000000	-3.152375000000
C	0.986784000000	-5.998380000000	-0.679519000000
H	0.390118000000	-6.387485000000	-1.530198000000
H	0.358978000000	-5.274800000000	-0.121865000000
H	1.234457000000	-6.846998000000	-0.007998000000
C	-1.593051000000	-0.343359000000	-2.924820000000
C	-1.971479000000	-0.876130000000	-4.162709000000
H	-1.223882000000	-1.381697000000	-4.794759000000
C	-3.309570000000	-0.760914000000	-4.576492000000
H	-3.632720000000	-1.177072000000	-5.542640000000
C	-4.232900000000	-0.105438000000	-3.741113000000
H	-5.277037000000	-0.018174000000	-4.083462000000
C	-3.883929000000	0.427611000000	-2.479714000000
C	-2.527169000000	0.284410000000	-2.053522000000
C	-6.850663000000	1.267427000000	-2.338255000000
H	-7.632285000000	1.758915000000	-1.721746000000
H	-7.198044000000	0.238098000000	-2.563217000000
H	-6.778507000000	1.823352000000	-3.295466000000
C	-5.449187000000	0.297555000000	0.218351000000
H	-4.488198000000	0.210686000000	0.763603000000
H	-5.818200000000	-0.726677000000	0.005281000000
H	-6.188152000000	0.806730000000	0.872267000000
C	-4.729370000000	3.062624000000	-1.030998000000
H	-5.488031000000	3.546571000000	-0.380452000000
H	-4.654091000000	3.642999000000	-1.973214000000
H	-3.745703000000	3.105296000000	-0.522345000000

Reference:

1. Hong, S.; Sutherlin, K. D.; Park, J.; Kwon, E.; Siegler, M. A.; Solomon, E. I.; Nam, W., Crystallographic and spectroscopic characterization and reactivities of a mononuclear non-haem iron(III)-superoxo complex. *Nat. Commun.* **2014,** *5*, 5440.
2. Cho, J.; Woo, J.; Nam, W., An "End-On" Chromium(III)-Superoxo Complex: Crystallographic and Spectroscopic Characterization and Reactivity in C−H Bond Activation of Hydrocarbons. *J. Am. Chem. Soc.* **2010,** *132* (17), 5958-5959.
3. Cramer, C. J.; Tolman, W. B.; Theopold, K. H.; Rheingold, A. L., Variable character of O-O and M-O bonding in side-on (η^2) 1:1 metal complexes of O_2. *Proc. Natl. Acad. Sci. U.S.A.* **2003,** *100* (7), 3635-3640.
4. Qin, K.; Incarvito, C. D.; Rheingold, A. L.; Theopold, K. H., A Structurally Characterized Chromium(III) Superoxide Complex Features "Side-on" Bonding. *Angew. Chem. Int. Ed.* **2002,** *41* (13), 2333-2335.
5. Yao, S.; Bill, E.; Milsmann, C.; Wieghardt, K.; Driess, M., A "Side-on" Superoxonickel Complex [LNi(O_2)] with a Square-Planar Tetracoordinate Nickel(II) Center and Its Conversion into [LNi(μ-OH)$_2$NiL]. *Angew. Chem. Int. Ed.* **2008,** *47* (37), 7110-7113.
6. Oddon, F.; Chiba, Y.; Nakazawa, J.; Ohta, T.; Ogura, T.; Hikichi, S., Characterization of Mononuclear Non-heme Iron (III)-Superoxo Complex with a Five-Azole Ligand Set. *Angew. Chem. Int. Ed.* **2015,** *54* (25), 7336-7339.
7. Würtele, C.; Gaoutchenova, E.; Harms, K.; Holthausen, M. C.; Sundermeyer, J.; Schindler, S., Crystallographic Characterization of a Synthetic 1:1 End-On Copper Dioxygen Adduct Complex. *Angew. Chem. Int. Ed.* **2006,** *45* (23), 3867-3869.
8. Iovan, D. A.; Wrobel, A. T.; McClelland, A. A.; Scharf, A. B.; Edouard, G. A.; Betley, T. A., Reactivity of a stable copper–dioxygen complex. *Chem. Commun.* **2017,** *53* (74), 10306-10309.
9. de Sousa, D. P.; Bigelow, J. O.; Sundberg, J.; Que, L.; McKenzie, C. J., Caught! Crystal trapping of a side-on peroxo bound to Cr(iv). *Chem. Commun.* **2015,** *51* (14), 2802-2805.
10. Yokoyama, A.; Han, J. E.; Cho, J.; Kubo, M.; Ogura, T.; Siegler, M. A.; Karlin, K. D.; Nam, W., Chromium(IV)–Peroxo Complex Formation and Its Nitric Oxide Dioxygenase Reactivity. *J. Am. Chem. Soc.* **2012,** *134* (37), 15269-15272.
11. Ramsey, C. M.; Cage, B.; Nguyen, P.; Abboud, K. A.; Dalal, N. S., Ligand Dependence of Magnetic Dimensionality in Chromium(IV) Complexes: Layered vs Three-Dimensional Antiferromagnets. *Chem. Mater.* **2003,** *15* (1), 92-99.
12. House, D. A.; Garner, C. S., Diperoxodiethylenetriamminechromium(IV) 1-hydrate: a New Chromium(IV) Peroxo Compound. *Nature* **1965,** *208* (5012), 776-777.

13. Annaraj, J.; Cho, J.; Lee, Y.-M.; Kim, S. Y.; Latifi, R.; de Visser, S. P.; Nam, W., Structural Characterization and Remarkable Axial Ligand Effect on the Nucleophilic Reactivity of a Nonheme Manganese(III)–Peroxo Complex. *Angew. Chem. Int. Ed.* **2009,** *48* (23), 4150-4153.
14. Lee, C.-M.; Chuo, C.-H.; Chen, C.-H.; Hu, C.-C.; Chiang, M.-H.; Tseng, Y.-J.; Hu, C.-H.; Lee, G.-H., Structural and Spectroscopic Characterization of a Monomeric Side-On Manganese(IV) Peroxo Complex. *Angew. Chem. Int. Ed.* **2012,** *51* (22), 5427-5430.
15. Singh, U. P.; Sharma, A. K.; Hikichi, S.; Komatsuzaki, H.; Moro-oka, Y.; Akita, M., Hydrogen bonding interaction between imidazolyl N–H group and peroxide: Stabilization of Mn(III)-peroxo complex $Tp^{iPr2}Mn(\eta^2\text{-}O_2)(im^{Me}H)$ ($im^{Me}H$=2-methylimidazole). *Inorg. Chim. Acta* **2006,** *359* (13), 4407-4411.
16. VanAtta, R. B.; Strouse, C. E.; Hanson, L. K.; Valentine, J. S., Peroxo(tetraphenylporphinato)manganese(III) and chloro(tetraphenylporphinato)manganese(II) anions. Synthesis, crystal structures, and electronic structures. *J. Am. Chem. Soc.* **1987,** *109* (5), 1425-1434.
17. Kang, H.; Cho, J.; Cho, K.-B.; Nomura, T.; Ogura, T.; Nam, W., Mononuclear Manganese–Peroxo and Bis(μ-oxo)dimanganese Complexes Bearing a Common N-Methylated Macrocyclic Ligand. *Chem. Eur. J.* **2013,** *19* (42), 14119-14125.
18. Seo, M. S.; Kim, J. Y.; Annaraj, J.; Kim, Y.; Lee, Y.-M.; Kim, S.-J.; Kim, J.; Nam, W., $[Mn(tmc)(O_2)]^+$: A Side-On Peroxido Manganese(III) Complex Bearing a Non-Heme Ligand. *Angew. Chem. Int. Ed.* **2007,** *46* (3), 377-380.
19. Colmer, H. E.; Geiger, R. A.; Leto, D. F.; Wijeratne, G. B.; Day, V. W.; Jackson, T. A., Geometric and electronic structure of a peroxomanganese(iii) complex supported by a scorpionate ligand. *Dalton Trans.* **2014,** *43* (48), 17949-17963.
20. Kitajima, N.; Komatsuzaki, H.; Hikichi, S.; Osawa, M.; Moro-oka, Y., A Monomeric Side-On Peroxo Manganese(III) Complex: $Mn(O_2)(3,5\text{-}^iPr_2pzH)(HB(3,5\text{-}^iPr_2pz)_3)$. *J. Am. Chem. Soc.* **1994,** *116* (25), 11596-11597.
21. Cho, J.; Jeon, S.; Wilson, S. A.; Liu, L. V.; Kang, E. A.; Braymer, J. J.; Lim, M. H.; Hedman, B.; Hodgson, K. O.; Valentine, J. S.; Solomon, E. I.; Nam, W., Structure and reactivity of a mononuclear non-haem iron(III)–peroxo complex. *Nature* **2011,** *478* (7370), 502-505.
22. Kishima, T.; Matsumoto, T.; Nakai, H.; Hayami, S.; Ohta, T.; Ogo, S., A High-Valent Iron(IV) Peroxo Core Derived from O_2. *Angew. Chem. Int. Ed.* **2016,** *55* (2), 724-727.
23. Rahman, A. F. M. M.; Jackson, W. G.; Willis, A. C., The First Sideways-Bonded Peroxo Complex for a Tetraaminecobalt(III) Species. *Inorg. Chem.* **2004,** *43* (24), 7558-7560.

24. Crump, D. B.; Stepaniak, R. F.; Payne, N. C., Charge distribution in dioxygen complexes of cobalt(III). The crystal structure and absolute configuration of (+)546-Δ-*cis*-*β*-[{2,13-dimethyl-6,9-diphenyl-2,6,9,13-tetraarsatetradecane}(dioxygen)cobalt(III)] perchlorate. *Can. J. Chem.* **1977,** *55* (3), 438-446.
25. Terry, N. W.; Amma, E. L.; Vaska, L., Molecular oxygen binding in a monomeric cobalt complex. Crystal and molecular structure of dioxygen-bis[*cis*-1,2-bis(diphenylphosphino)ethylene]cobalt tetrafluoroborate. *J. Am. Chem. Soc.* **1972,** *94* (2), 653-655.
26. Halpern, J.; Goodall, B. L.; Khare, G. P.; Lim, H. S.; Pluth, J. J., Reaction of oxygen with dicyanotris(dimethylphenylphosphine)cobalt(II). Synthesis, structure, and reactivity of a novel cobalt-dioxygen adduct. *J. Am. Chem. Soc.* **1975,** *97* (8), 2301-2303.
27. Hu, X.; Castro-Rodriguez, I.; Meyer, K., Dioxygen Activation by a Low-Valent Cobalt Complex Employing a Flexible Tripodal N-Heterocyclic Carbene Ligand. *J. Am. Chem. Soc.* **2004,** *126* (41), 13464-13473.
28. DeRosha, D. E.; Mercado, B. Q.; Lukat-Rodgers, G.; Rodgers, K. R.; Holland, P. L., Enhancement of C−H Oxidizing Ability in Co–O_2 Complexes through an Isolated Heterobimetallic Oxo Intermediate. *Angew. Chem. Int. Ed.* **2017,** *56* (12), 3211-3215.
29. Cho, J.; Sarangi, R.; Kang, H. Y.; Lee, J. Y.; Kubo, M.; Ogura, T.; Solomon, E. I.; Nam, W., Synthesis, Structural, and Spectroscopic Characterization and Reactivities of Mononuclear Cobalt(III)−Peroxo Complexes. *J. Am. Chem. Soc.* **2010,** *132* (47), 16977-16986.
30. Schaefer, W. P.; Huie, B. T.; Kurilla, M. G.; Ealick, S. E., Oxygen-carrying cobalt complexes. 10. Structures of N,N'-ethylenebis(3-tert-butylsalicylideniminato)cobalt (II) and its monomeric dioxygen adduct. *Inorg. Chem.* **1980,** *19* (2), 340-344.
31. Zhang, Q.; Bell-Taylor, A.; Bronston, F. M.; Gorden, J. D.; Goldsmith, C. R., Aldehyde Deformylation and Catalytic C–H Activation Resulting from a Shared Cobalt(II) Precursor. *Inorg. Chem.* **2017,** *56* (2), 773-782.
32. Noh, H.; Jeong, D.; Ohta, T.; Ogura, T.; Valentine, J. S.; Cho, J., Distinct Reactivity of a Mononuclear Peroxocobalt(III) Species toward Activation of Nitriles. *J. Am. Chem. Soc.* **2017,** *139* (32), 10960-10963.
33. Kim, J.; Shin, B.; Kim, H.; Lee, J.; Kang, J.; Yanagisawa, S.; Ogura, T.; Masuda, H.; Ozawa, T.; Cho, J., Steric Effect on the Nucleophilic Reactivity of Nickel(III) Peroxo Complexes. *Inorg. Chem.* **2015,** *54* (13), 6176-6183.
34. Cho, J.; Kang, H. Y.; Liu, L. V.; Sarangi, R.; Solomon, E. I.; Nam, W.,

Mononuclear nickel(ii)-superoxo and nickel(iii)-peroxo complexes bearing a common macrocyclic TMC ligand. *Chem. Sci.* **2013,** *4* (4), 1502-1508.

35. Cho, J.; Sarangi, R.; Annaraj, J.; Kim, S. Y.; Kubo, M.; Ogura, T.; Solomon, E. I.; Nam, W., Geometric and electronic structure and reactivity of a mononuclear 'side-on' nickel(iii)–peroxo complex. *Nat. Chem.* **2009,** *1* (7), 568-572.
36. Aboelella, N. W.; Kryatov, S. V.; Gherman, B. F.; Brennessel, W. W.; Young, V. G.; Sarangi, R.; Rybak-Akimova, E. V.; Hodgson, K. O.; Hedman, B.; Solomon, E. I.; Cramer, C. J.; Tolman, W. B., Dioxygen Activation at a Single Copper Site: Structure, Bonding, and Mechanism of Formation of 1:1 Cu−O_2 Adducts. *J. Am. Chem. Soc.* **2004,** *126* (51), 16896-16911.
37. Aboelella, N. W.; Lewis, E. A.; Reynolds, A. M.; Brennessel, W. W.; Cramer, C. J.; Tolman, W. B., Snapshots of Dioxygen Activation by Copper: The Structure of a 1:1 Cu/O_2 Adduct and Its Use in Syntheses of Asymmetric Bis(μ-oxo) Complexes. *J. Am. Chem. Soc.* **2002,** *124* (36), 10660-10661.
38. Reynolds, A. M.; Gherman, B. F.; Cramer, C. J.; Tolman, W. B., Characterization of a 1:1 Cu−O2 Adduct Supported by an Anilido Imine Ligand. *Inorg. Chem.* **2005,** *44* (20), 6989-6997.
39. Egan Jr, J. W.; Haggerty, B. S.; Rheingold, A. L.; Sendlinger, S. C.; Theopold, K. H., Crystal Structure of a Side-On Superoxo Complex of Cobalt and Hydrogen Abstraction by a Reactive Terminal Oxo Ligand. *J. Am. Chem. Soc.* **1990,** *112* (6), 2445-2446.
40. Fujisawa, K.; Tanaka, M.; Moro-oka, Y.; Kitajima, N., A Monomeric Side-On Superoxocopper(II) Complex: Cu(O_2)(HB(3-tBu-5-iPrpz)$_3$). *J. Am. Chem. Soc.* **1994,** *116* (26), 12079-12080.
41. Kieber-Emmons, M. T.; Annaraj, J.; Seo, M. S.; Van Heuvelen, K. M.; Tosha, T.; Kitagawa, T.; Brunold, T. C.; Nam, W.; Riordan, C. G., Identification of an "End-on" Nickel−Superoxo Adduct, [Ni(tmc)(O_2)]$^+$. *J. Am. Chem. Soc.* **2006,** *128* (44), 14230-14231.
42. Panda, C.; Chandra, A.; Corona, T.; Andris, E.; Pandey, B.; Garai, S.; Lindenmaier, N.; Künstner, S.; Farquhar, E. R.; Roithová, J., Nucleophilic Versus Electrophilic Reactivity of Bioinspired Superoxido Nickel(II) Complexes. *Angew. Chem. Int. Ed.* **2018,** *130* (45), 15099-15103.
43. Wang, C.-C.; Chang, H.-C.; Lai, Y.-C.; Fang, H.; Li, C.-C.; Hsu, H.-K.; Li, Z.-Y.; Lin, T.-S.; Kuo, T.-S.; Neese, F.; Ye, S.; Chiang, Y.-W.; Tsai, M.-L.; Liaw, W.-F.; Lee, W.-Z., A Structurally Characterized Nonheme Cobalt–Hydroperoxo Complex Derived from Its Superoxo Intermediate via Hydrogen Atom Abstraction. *J. Am. Chem. Soc.* **2016,** *138* (43), 14186-14189.
44. Chiang, C.-W.; Kleespies, S. T.; Stout, H. D.; Meier, K. K.; Li, P.-Y.; Bominaar,

E. L.; Que Jr, L.; Münck, E.; Lee, W.-Z., Characterization of a Paramagnetic Mononuclear Nonheme Iron-Superoxo Complex. *J. Am. Chem. Soc.* **2014,** *136* (31), 10846-10849.

45. Lin, Y.-H.; Cramer, H. H.; van Gastel, M.; Tsai, Y.-H.; Chu, C.-Y.; Kuo, T.-S.; Lee, I. R.; Ye, S.; Bill, E.; Lee, W.-Z., Mononuclear Manganese(III) Superoxo Complexes: Synthesis, Characterization, and Reactivity. *Inorg. Chem.* **2019,** *58* (15), 9756-9765.
46. Fischer, A. A.; Lindeman, S. V.; Fiedler, A. T., Spectroscopic and computational studies of reversible O_2 binding by a cobalt complex of relevance to cysteine dioxygenase. *Dalton Trans.* **2017,** *46* (39), 13229-13241.
47. Fischer, A. A.; Lindeman, S. V.; Fiedler, A. T., A synthetic model of the nonheme iron–superoxo intermediate of cysteine dioxygenase. *Chem. Commun.* **2018,** *54* (80), 11344-11347.
48. Maiti, D.; Fry, H. C.; Woertink, J. S.; Vance, M. A.; Solomon, E. I.; Karlin, K. D., A 1:1 Copper−Dioxygen Adduct is an End-on Bound Superoxo Copper(II) Complex which Undergoes Oxygenation Reactions with Phenols. *J. Am. Chem. Soc.* **2007,** *129* (2), 264-265.
49. Kunishita, A.; Kubo, M.; Sugimoto, H.; Ogura, T.; Sato, K.; Takui, T.; Itoh, S., Mononuclear Copper(II)−Superoxo Complexes that Mimic the Structure and Reactivity of the Active Centers of PHM and D*β*M. *J. Am. Chem. Soc.* **2009,** *131* (8), 2788-2789.
50. Gordon, J. B.; Vilbert, A. C.; Siegler, M. A.; Lancaster, K. M.; Moënne-Loccoz, P.; Goldberg, D. P., A Nonheme Thiolate-Ligated Cobalt Superoxo Complex: Synthesis and Spectroscopic Characterization, Computational Studies, and Hydrogen Atom Abstraction Reactivity. *J. Am. Chem. Soc.* **2019,** *141* (8), 3641-3653.
51. McNeece, A. J.; Jesse, K. A.; Xie, J.; Filatov, A. S.; Anderson, J. S., Generation and Oxidative Reactivity of a Ni(II) Superoxo Complex via Ligand-Based Redox Non-Innocence. *J. Am. Chem. Soc.* **2020,** *142* (24), 10824-10832.
52. Kim, H.; Rogler, P. J.; Sharma, S. K.; Schaefer, A. W.; Solomon, E. I.; Karlin, K. D., Heme-Fe^{III} Superoxide, Peroxide and Hydroperoxide Thermodynamic Relationships: Fe^{III}-$O_2^{\bullet-}$ Complex H-Atom Abstraction Reactivity. *J. Am. Chem. Soc.* **2020,** *142* (6), 3104-3116.
53. Bhadra, M.; Transue, W. J.; Lim, H.; Cowley, R. E.; Lee, J. Y. C.; Siegler, M. A.; Josephs, P.; Henkel, G.; Lerch, M.; Schindler, S.; Neuba, A.; Hodgson, K. O.; Hedman, B.; Solomon, E. I.; Karlin, K. D., A Thioether-Ligated Cupric Superoxide Model with Hydrogen Atom Abstraction Reactivity. *J. Am. Chem. Soc.* **2021,** *143* (10), 3707-3713.

54. Kim, H.; Sharma, S. K.; Schaefer, A. W.; Solomon, E. I.; Karlin, K. D., Heme–Cu Binucleating Ligand Supports Heme/O2 and FeII–CuI/O2 Reactivity Providing High- and Low-Spin FeIII–Peroxo–CuII Complexes. *Inorg. Chem.* **2019,** *58* (22), 15423-15432.
55. Sharma, S. K.; Schaefer, A. W.; Lim, H.; Matsumura, H.; Moënne-Loccoz, P.; Hedman, B.; Hodgson, K. O.; Solomon, E. I.; Karlin, K. D., A Six-Coordinate Peroxynitrite Low-Spin Iron(III) Porphyrinate Complex—The Product of the Reaction of Nitrogen Monoxide (·NO(g)) with a Ferric-Superoxide Species. *J. Am. Chem. Soc.* **2017,** *139* (48), 17421-17430.
56. Kim, E.; Helton, M. E.; Wasser, I. M.; Karlin, K. D.; Lu, S.; Huang, H.-w.; Moënne-Loccoz, P.; Incarvito, C. D.; Rheingold, A. L.; Honecker, M.; Kaderli, S.; Zuberbühler, A. D., Superoxo, μ-peroxo, and μ-oxo complexes from heme/O₂ and heme-Cu/O₂ reactivity: Copper ligand influences in cytochrome c oxidase models. *Proc. Natl. Acad. Sci. U.S.A.* **2003,** *100* (7), 3623.
57. Wasser, I. M.; Huang, H.-w.; Moënne-Loccoz, P.; Karlin, K. D., Heme/Non-Heme Diiron(II) Complexes and O2, CO, and NO Adducts as Reduced and Substrate-Bound Models for the Active Site of Bacterial Nitric Oxide Reductase. *J. Am. Chem. Soc.* **2005,** *127* (10), 3310-3320.
58. Das, P. K.; Mittra, K.; Dey, A., Spectroscopic characterization of a phenolate bound FeII–O2 adduct: gauging the relative "push" effect of a phenolate axial ligand. *Chem. Commun.* **2014,** *50* (40), 5218-5220.
59. Mittra, K.; Chatterjee, S.; Samanta, S.; Sengupta, K.; Bhattacharjee, H.; Dey, A., A hydrogen bond scaffold supported synthetic heme FeIII–O2− adduct. *Chem. Commun.* **2012,** *48* (85), 10535-10537.
60. Kim, S.; Lee, J. Y.; Cowley, R. E.; Ginsbach, J. W.; Siegler, M. A.; Solomon, E. I.; Karlin, K. D., A N3S(thioether)-Ligated CuII-Superoxo with Enhanced Reactivity. *J. Am. Chem. Soc.* **2015,** *137* (8), 2796-2799.
61. Lee, J. Y.; Peterson, R. L.; Ohkubo, K.; Garcia-Bosch, I.; Himes, R. A.; Woertink, J.; Moore, C. D.; Solomon, E. I.; Fukuzumi, S.; Karlin, K. D., Mechanistic Insights into the Oxidation of Substituted Phenols via Hydrogen Atom Abstraction by a Cupric–Superoxo Complex. *J. Am. Chem. Soc.* **2014,** *136* (28), 9925-9937.
62. Ginsbach, J. W.; Peterson, R. L.; Cowley, R. E.; Karlin, K. D.; Solomon, E. I., Correlation of the Electronic and Geometric Structures in Mononuclear Copper(II) Superoxide Complexes. *Inorg. Chem.* **2013,** *52* (22), 12872-12874.
63. Bhadra, M.; Lee, J. Y. C.; Cowley, R. E.; Kim, S.; Siegler, M. A.; Solomon, E. I.; Karlin, K. D., Intramolecular Hydrogen Bonding Enhances Stability and Reactivity of Mononuclear Cupric Superoxide Complexes. *J. Am. Chem. Soc.* **2018,** *140* (29),

9042-9045.

64. Peterson, R. L.; Himes, R. A.; Kotani, H.; Suenobu, T.; Tian, L.; Siegler, M. A.; Solomon, E. I.; Fukuzumi, S.; Karlin, K. D., Cupric Superoxo-Mediated Intermolecular C−H Activation Chemistry. *J. Am. Chem. Soc.* **2011,** *133* (6), 1702-1705.
65. Diaz, D. E.; Quist, D. A.; Herzog, A. E.; Schaefer, A. W.; Kipouros, I.; Bhadra, M.; Solomon, E. I.; Karlin, K. D., Impact of Intramolecular Hydrogen Bonding on the Reactivity of Cupric Superoxide Complexes with O−H and C−H Substrates. *Angew. Chem. Int. Ed.* **2019,** *58* (49), 17572-17576.
66. Donoghue, P. J.; Gupta, A. K.; Boyce, D. W.; Cramer, C. J.; Tolman, W. B., An Anionic, Tetragonal Copper(II) Superoxide Complex. *J. Am. Chem. Soc.* **2010,** *132* (45), 15869-15871.